This article has been accepted for publication in IEEE Journal of Selected Topics in Quantum Electronics. This is the author's version which has not been fully edited and content may change prior to final publication. Citation information: DOI 10.1109/JSTQE.2025.3641548

InAs/InAlGaAs Quantum Dot Lasers on InP and Si

Hui Jia, Jae-Seong Park, Jun Li, Kongming Liu, Jiajing Yuan, Calum Dear, Haotian Zeng, Yangqian Wang, Khalil El Hajraoui, Shangfeng Liu, Huiwen Deng, Mickael Martin, Yaonan Hou, Quentin M. Ramasse, Richard Beanland, Qiang Li, Thierry Baron, Mingchu Tang, Alwyn Seeds, and Huiyun Liu

(Invited Paper)

***Abstract*—We report the development of InAs/InAlGaAs quantum-dot (QD) lasers grown on both InP and Si substrates. A modified indium flush technique was employed to control dot-height distribution and tailor the emission wavelength by using a strained partial capping layer. Using this approach, 7-stack InAs/InAlGaAs QD lasers on InP substrates exhibit a low threshold current density (J_{th}) of 63 A/cm^2 per QD layer and high-temperature operation up to 140 °C. Furthermore, electrically pumped InAs/InAlGaAs QD lasers directly grown on Si are also demonstrated, with a low J_{th} of 1.35 kA/cm^2 and a maximum operating temperature of 100 °C. This work highlights the effectiveness of the modified indium flush in achieving high-performance InAs/InAlGaAs QD lasers. These results represent a significant step forward in the development of high-performance C-/L-band QD lasers in the InAs/InAlGaAs/InP material system for Si photonics.**

***Index Terms*—Quantum dots, semiconductor lasers, indium flush, InAs/InAlGaAs, molecular beam epitaxy.**

This paper was submitted at xx. This work was supported in part by the UK Engineering and Physical Sciences Research Council under Grants EP/V029606/1, EP/V029681/1, EP/Z532848/1, EP/X015300/1, EP/T028475/1, EP/S024441/1, EP/X035123/1, EP/W021080/1, and EP/P006973/1); European Union's Horizon 2020 program (101129904). *(Corresponding author: Mingchu Tang; Huiyun Liu).* Hui Jia and Jae-Seong Park contributed equally to this work.

Hui Jia, Jae-Seong Park, Jun Li, Kongming Liu, Jiajing Yuan, Calum Dear, Haotian Zeng, Yangqian Wang, Huiwen Deng, Mingchu Tang, Alwyn Seeds and Huiyun Liu are with the Department of Electronic and Electrical Engineering, University College London, London WC1E 7JE, UK. (E-mail: hui.jia@ucl.ac.uk; jae-seong.park@ucl.ac.uk; jun.li.21@ucl.ac.uk; kongming.liu.20@ucl.ac.uk; jiajing.yuan.17@ucl.ac.uk; calum.dear.20@ucl.ac.uk; fiona.wang@ucl.ac.uk; haotian.zeng@ucl.ac.uk; huiwen.deng@ucl.ac.uk; mingchu.tang@ucl.ac.uk; a.seeds@ucl.ac.uk; huiyun.liu@ucl.ac.uk)

Khalil EI Hajraoui is with the SuperSTEM, SciTech Daresbury Science and Innovation Campus, Block J, Keckwick Lane, Daresbury, WA4 4AD, UK and York NanoCentre & Department of Physics, University of York, York, YO10 5DD, UK. (E-mail: kelhajraoui@superstem.org).

Quentin M. Ramasse is with the SuperSTEM, SciTech Daresbury Science and Innovation Campus, Block J, Keckwick Lane, Daresbury, WA4 4AD, UK and School of Chemical and Process Engineering and School of Physics and Astronomy, University of Leeds, Leeds, LS2 9JT, UK. (E-mail: qmramasse@superstem.org)

Shangfeng Liu and Qiang Li are with the School of Physics and Astronomy, Cardiff University, Cardiff CF24 3AA, UK. (E-mail: sfliu@gbu.edu.cn; LiQ44@cardiff.ac.uk)

Mickael Martin and Thierry Baron are with the University Grenoble Alpes, CNRS, CEA/LETI-Minatec, Grenoble INP, LTM, Grenoble F-38054, France. (E-mail: mickael.martin@cea.fr; thierry.baron@cea.fr)

Yaonan Hou is with the Department of Electronic and Electrical Engineering, Bay Campus, Swansea University, Swansea, SA1 8EN, UK and Centre for Integrative Semiconductor Materials (CISM), Swansea University, Bay Campus, SA1 8EN, Swansea, UK. (E-mail: yaonan.hou@swansea.ac.uk)

Richard Beanland is with the Department of Physics, University of Warwick, Gibbet Hill, Coventry, CV4 7AL, UK. (E-mail: r.beanland@warwick.ac.uk)

I. INTRODUCTION

High-performance semiconductor lasers operating in the C- and L-band wavelengths are of great importance for modern optical communication systems applied in data center and Si photonics [1-3]. Furthermore, amid the rise of artificial intelligence and big data, light sources compatible with large-scale photonic integration are urgently required to tackle the surging bandwidth and energy consumption [4]. In particular, light sources that can be monolithically integrated onto Si platforms are considered key elements for next-generation electronic and photonic integrated circuits for artificial intelligence and big data [5].

Quantum-dot (QD) lasers have emerged as a promising candidate for such applications, offering various advantages over conventional quantum well lasers [6-8]. Their three-dimensional carrier confinement leads to a discrete energy state, resulting in low threshold current density (J_{th}), nearly-zero linewidth enhancement factor, ultra-fast gain dynamics, high temperature operation, *etc* [6, 9-14]. Furthermore, the strong carrier localization in QDs provides defect tolerance, making them suitable for monolithic integration on Si substrates, which inevitably suffer from high density of defects during the heteroepitaxy [15-18].

Although InAs/InAlGaAs QD lasers are promising candidates for C- and L-band light sources, their development has been hampered by epitaxial growth challenges. One of the primary obstacles in InAs/InP material system is the anisotropic indium diffusion coefficient along [110] and [1$\bar{1}$0] directions on an InP (001) substrate, leading to the formation of elongated quantum dash (Qdash) structures along the [1$\bar{1}$0] direction, which disrupts the desired three-dimensional carrier confinement and undermines many benefits of QDs [9, 19-21]. Additionally, the broader dot-size distributions induced by moderate lattice mismatch (~ 3.2 %) between InAs and InP result in significant inhomogeneous spectral broadening, which limits modal gain and hinders the realization of high-performance InAs/InAlGaAs QD lasers [6, 22, 23].

Over the past two decades, a great deal of effort has been made to improve the size/shape uniformity of InAs/InAlGaAs QDs. Various growth strategies have been explored, including the adjustments to growth temperature, V/III ratio, growth rate, growth interruption and use of As_2 instead of As_4 [19, 24-26]. These aim at accelerating the dot formation process and thereby suppressing the anisotropic surface diffusion of indium. Furthermore, modifications to the underlying layer composition, such as InAlAs, InGaAs, AlGaAs, GaAs or

InAlGaAs, have been employed to control the growth front, strain field, and phase separation, thereby optimizing QD nucleation and morphology [19, 27-31].

As an alternative solution, the indium flush technique controls the dot-height uniformity and tunes the emission wavelength [32-37]. This involves partially capping the QDs with a thin first capping layer (FCL), followed by annealing at elevated temperature to evaporate the indium or to induce an As/P exchange process, which reduces the height of large dots. A subsequent second capping layer (SCL) is then grown to complete the structure. Most dots present a similar height as the FCL, leading to a significant blueshift in emission wavelength and a narrower full-width at half-maximum (FWHM) of photoluminescence (PL). For example, Luo *et al*. demonstrated a peak wavelength blueshift from 1690 nm to 1570 nm and a PL FWHM reduction from 124 meV to 87 meV for 5-stacked InAs/InGaAsP QDs, by using an optimal SCL growth temperature that maximizes the indium migration and As/P exchange reaction [34]. Our previous work optimized the FCL thickness and annealing temperature, achieving a narrow PL FWHM of 50.9 meV for a 5-layer InAs/InAlGaAs QD stack [32]. However, the employment of the indium flush technique in the InAs/InAlGaAs/InP QD system remains relatively underexplored, particularly with varied composition of FCL and thickness adjustment for FCL/SCL combinations.

Furthermore, there is a growing demand toward realizing monolithic InAs/InAlGaAs QD lasers on Si as an on-chip light source for Si photonics, because QDs are less sensitive to defects generated from the interface between III-V and Si [15, 38, 39]. While O-band InAs/GaAs QD lasers have shown substantial advances in monolithic integration on Si platforms, the situation for the C-/L-band InAs/InAlGaAs QD lasers is more complex. The large lattice mismatch of ~ 8% between InP and Si (~ 4% for GaAs and Si) results in much higher densities of threading dislocation, as well as antiphase boundaries and thermal cracks [40, 41]. These issues make the direct growth of electrically pumped InAs/InAlGaAs QD lasers on Si (001) extremely difficult, and only a few reports have demonstrated such devices to date [42, 43]. For instance, Zhu *et al*. [42] reported pulsed InAs/InAlGaAs QD lasers on Si with J_{th} of 1.6 kA/cm^2, total output power of 110 mW, and maximum operating temperature of 80 °C, using InGaAs/InP defect filter layer and V-groove patterned (001) Si.

In this work, we present an epitaxial approach to develop InAs/InAlGaAs QD lasers on both InP and Si substrates. The QD active regions were grown by molecular beam epitaxy (MBE) as its sub-monolayer precision and solid-source evaporation offer superior control over interface abruptness and stoichiometry compared to metal-organic chemical vapor deposition (MOCVD), where gas-phase reactions can introduce variability. We first examine a modified indium flush technique, utilizing a strained InAlGaAs layer as part of the FCL and varying strained/unstrained FCL thickness combination, to improve dot height uniformity and control emission wavelength. This growth strategy is then used to fabricate 7-stack InAs/InAlGaAs QD lasers on (001) InP substrates, demonstrating high-performance lasers with low J_{th} and high-temperature operation. This technique is further exploited to grow InAs/InAlGaAs QD lasers directly on Si (001) substrates. Lasing operation up to 100 ºC is demonstrated for InAs/InAlGaAs QD lasers directly grown on Si with a low J_{th} of 1.35 kA/cm^2 at room temperature (RT). These results represent significant progress in InAs/InAlGaAs QD laser development and highlight the potential for InP- and Si-based InAs/InAlGaAs QD lasers in optical communication and Si photonics.

II. EXPERIMENT

All the active regions of the InAs/InAlGaAs QD samples were grown by solid-source MBE system equipped with a valved arsenic cracker source on InP (001) and Si (001) substrates. Prior to growth, the substrates were degassed in the buffer chamber at 400 °C for an hour and then transferred to the growth chamber for a 1-min deoxidation at 500 °C under As_2 overpressure. The detailed growth information regarding InAs/InAlGaAs QDs will be presented in each respective section. Scanning transmission electron microscopy (STEM) was performed to investigate the cross-sectional structural characteristics. In addition, atomic force microscopy (AFM) was employed to examine the surface morphology of QD samples, enabling direct comparison before and after stacking. PL measurements at RT were conducted using a Nanometrics RPM2000 system, incorporating a 635 nm continuous-wave laser at an excitation power density of 430 W/cm² and a wavelength-extended InGaAs detector with a cutoff at 2 μm.

Fabry-Pérot (FP) lasers were fabricated on both InP and Si substrates. Ridges were formed slightly above the active region by conventional photolithography and wet chemical etch using a mixture of HCl and H_3PO_4. For Si-based lasers, an additional wet etch step was employed to form a second mesa structure and expose the n-type InP contact layer for a top-top contact configuration. After the ridge formation, a 400 nm SiO_2 passivation layer was deposited by plasma-enhanced chemical vapor deposition, and contact windows were opened by reactive ion etching. Ti/Au (20/400 nm) was deposited on the exposed ridge using a sputtering system as the p-contact. For InP-based lasers, substrates were thinned to 150 μm and subsequently, an n-type Ni/AuGe/Ni/Au (10/100/10/200 nm) contact layer was deposited on the polished surface using a thermal evaporator. For Si-based lasers, the same n-type metallization was first deposited on the exposed n-type InP contact layer, followed by substrate thinning to 150 μm. Both were annealed at 380 °C for 1 min to form ohmic contacts. No facet coating was applied.

III. INDIUM FLUSH FOR INAS/INALGAAS QD GROWTH

A. Mechanism Revealed by STEM Investigations

While indium flush has been widely applied to InAs/GaAs QD growth to manipulate the dot uniformity and hence enhance gain [44-46], its adoption in InAs/InAlGaAs/InP material system remains less explored, especially in the quaternary alloy barrier matrices. Therefore, we studied the mechanism of indium flush in an InAs/InAlGaAs material system. Two single-layer QD samples were grown to study the effect of

indium flush, of which the growth parameters were discussed in our previous work [32]. Reference sample A (without indium flush) consists of 500 nm InAlAs and 100 nm InAlGaAs grown on an n-type InP (001) substrate. 5.5 monolayers (MLs) of InAs were deposited directly onto InAlGaAs at 485 °C with a V/III ratio of 18, followed by a 10-second growth interruption under As overpressure to promote QD ripening [26]. A 100 nm InAlGaAs capping layer was then deposited at the same temperature. Additional 100 nm InAlAs, 100 nm InAlGaAs, and surface QDs were grown sequentially to complete the reference sample for PL measurements. A high indium growth rate of 0.42 ML/s and As_2 were used for the QD growth to suppress the anisotropic indium surface diffusion. All layers except the InAs QD layer are lattice-matched to InP. Sample B (with indium flush) was grown under identical conditions except that after the QD deposition and growth interruption, a 4-nm InAlGaAs FCL was grown at 485 °C. Then, the substrate temperature was increased to 540 °C and held for 1 min under As_2 flux with a beam equivalent pressure of 7×10^{-6} Torr (the indium flush step), followed by the growth of the remaining 96 nm InAlGaAs SCL at 500 °C [47]. The emission wavelength was blue shifted by over 300 nm from 1824 nm for sample A to 1522 nm for sample B, and the PL FWHM improved significantly from 89.2 to 47.9 meV. High-angle annular-dark-field (HAADF) STEM images of sample A and B are presented in Fig. 1 (a) and (b), respectively. For sample A without indium flush, a large QD size dispersion is observed, with a mean QD height of 5.46 ± 0.84 nm. In contrast, the QDs in sample B with indium flush are clearly truncated, with a reduced average height of 3.54 ± 0.48 nm, as the larger dots are affected by the flush while smaller dots are fully buried. This facilitates the size quantization-assisted blue shift and improves the uniformity of the dot ensemble dramatically.

Apart from the QD height modifications, HAADF images of sample B also show dark-contrasted regions connecting adjacent dots and bright-contrasted regions above large, truncated dots. Electron energy loss spectroscopy (EELS) measurements confirm these to be Al-rich and In-rich regions, respectively, as seen in Figure 1 (c) and (d). Based on these distinctive observations, we propose a growth model, as shown in Fig. 1 (e – j). Initially, QDs form via Stranski-Krastanov growth mode. Then, the 4 nm quaternary InAlGaAs FCL is deposited; as the average dot height is 5.46 ± 0.84 nm, only larger dots (> 4 nm) remain exposed while smaller dots (< 4 nm) are buried. The elastically relaxed InAs island apices of exposed QDs create energetically unfavorable nucleation sites for Ga and Al adatoms, thereby limiting the FCL growth atop the QDs [22, 44, 46-48]. Strain from the InAlGaAs FCL promotes indium migration across the FCL surface, forming a partial capping layer to reduce the surface energy [44]. Upon substrate temperature elevation, indium desorbs from both the partially capped dot layer and the FCL, leaving the top of the FCL Al-rich, thereby accounting for the dark-contrasted regions between adjacent dots in atomic-number-sensitive STEM-HAADF images. During the subsequent SCL growth, indium atoms readily incorporate above the truncated dots because of the smaller lattice mismatch, i.e. less compressive strain, forming In-rich regions above truncated dots as shown in Fig. 1(b).

These findings offer important insight into the complex dynamics occurring during the indium flush process in quaternary material matrices, thereby contributing to the further optimization and broader applicability of this technique.

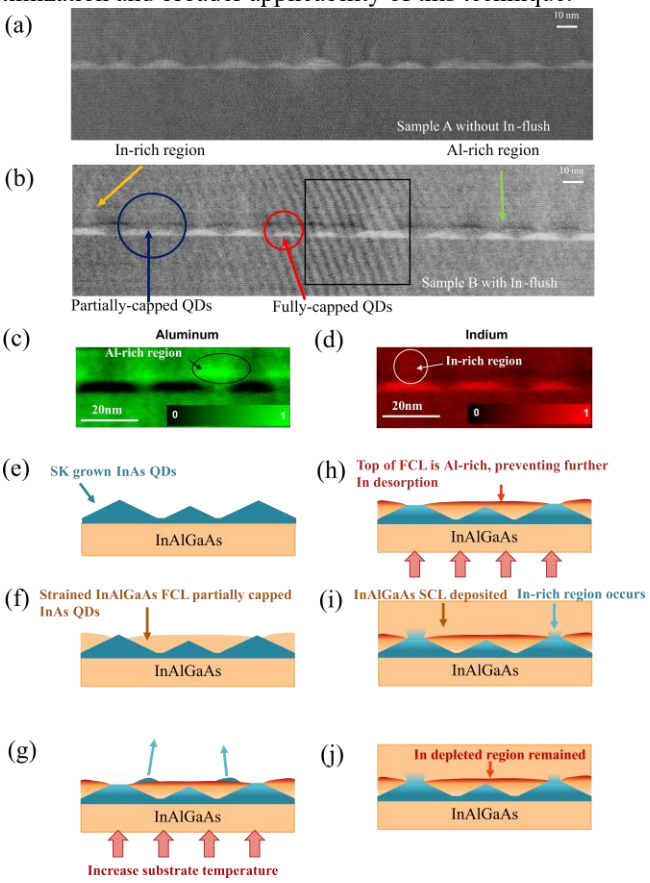

Fig. 1. HAADF images of QD morphologies and adjacent layers of sample A (without indium flush) in (a) and sample B (with indium flush) in (b). (c) and (d) Individual EELS maps of sample B, showing the relative distribution of Al (green intensity channel) and In (red intensity channel). (e – j) The schematic illustration of the proposed impact of the indium flush technique on QDs and adjacent regions. (e) Formation of InAs QDs. (f) The deposition of FCL. (g) The substrate temperature is elevated, and indium atoms desorb from both FCL and QDs. (h) Desorbed indium atoms are flushed away. (i) Indium-rich region and (j) indium-depleted (Al-rich) region formed after the deposition of SCL (Adapted from [47] under CC BY 4.0).

B. Modified Indium Flush Technique

More flexibility is given to optimizing the growth condition for high density and uniform QDs due to the capability of indium flush to effectively tune the emission wavelength and QD height uniformity. Theoretically, increasing the InAs deposition thickness leads to a shape transition from elongated QD dashes to round-shaped islands, hence increasing QD density [8]. Consequently, to increase QD density, we further increased the InAs thickness based on previous work [32]. High QD densities of 4.4×10^{10} cm^{-2} and 5.2×10^{10} cm^{-2} were

achieved by an InAs coverage of 6.5 MLs and 6.8 MLs, respectively. However, the emission wavelength also increases with increasing InAs coverage [32]. For the sample with 6.5 ML InAs coverage, even using indium flush technique with an unstrained InAlGaAs FCL of 3.5 nm, the emission wavelength is still as long as 1726 nm.

To further shift the emission wavelength to within the C-/L-band, we developed a modified indium flush technique that utilized a strained InAlGaAs layer as part of the FCL. By changing the thickness of the strained $In_{0.359}Al_{0.323}Ga_{0.318}As$ FCL, which has a smaller lattice parameter than InP, significant blue shift in PL peak wavelength can be achieved. Three samples with different FCL were grown to investigate the capability of wavelength tuning. The schematic QD structure is shown in Fig. 2(a). For sample R1, after the 6.5 ML QD growth and interruption for 10 seconds at 485 °C, a 0.5-nm strained $In_{0.359}Al_{0.323}Ga_{0.318}As$ layer and a 2-nm $In_{0.528}Al_{0.238}Ga_{0.234}As$ layer were subsequently deposited on the QDs as the FCL. Then the thermal annealing was carried out at 515 °C for 3 min and the remaining 97.5-nm $In_{0.528}Al_{0.238}Ga_{0.234}As$ SCL growth resumed at 485 °C. Note that the difference in annealing temperature compared with that in Section III-A is due to the variations in the different facility setup. For sample R2, the FCL consisted of 1.5 nm strained $In_{0.359}Al_{0.323}Ga_{0.318}As$ and 1 nm $In_{0.528}Al_{0.238}Ga_{0.234}As$ and R3 is a reference sample with unstrained FCL. It should be noted that in our experiment, the stressor layer was grown directly on top of QDs rather than in the second part of the FCL because this should have an immediate impact on the strain field within and around the dots, which more readily affects the indium flush procedure and the material exchange at the interface. The PL spectra of the three samples are shown in Fig. 2(b). The inset in Fig. 2(b) shows a 1×1 μm^2 AFM image of the uncapped surface dots of the samples with highly uniform and high density QDs. A significant blue shift from 1624.8 nm to 1576.2 nm is obtained just by changing the strained $In_{0.359}Al_{0.323}Ga_{0.318}As$ layer thickness by 1 nm from R1 to R2. The effectiveness of using lower composition InAlGaAs FCL in tuning emission wavelength is also reported by Kwoen *et al.* [49], thanks to the band energy modification and reduced indium interdiffusion during subsequent annealing process. In addition, a 27% enhancement in PL intensity is achieved for the sample with 0.5 nm strained $In_{0.359}Al_{0.323}Ga_{0.318}As$. The reduction in strain in the FCL and the spacer layer brought by this strained InAlGaAs is reported to affect the interdiffusion of indium atoms at the InAs/InAlGaAs interface [50], which might account for the observed improvement in PL intensity. Compared to the reference sample, the peak wavelength of the sample with 1.5 nm strained InAlGaAs is blue shifted significantly by 150 nm. The FWHM of the strained InAlGaAs samples shows a slight decrease (58.2 meV for R1 and 58.3 meV for R2) compared to the reference sample (59 meV).

This modified indium flush technique not only effectively shifts the emission wavelength, thus allowing more flexibility for QD growth optimization, but is also especially advantageous for multi-layer QD stack growth due to the strain compensation effect [35, 51]. More QD stacks and thinner spacer layers can be expected using this technique, which favors the growth of high gain, low defect density QDs. In the following sections, multi-layer InAs/InAlGaAs/InP QD lasers based on this modified indium flush have been developed and demonstrated high performance in terms of high-temperature operation and low J_{th}.

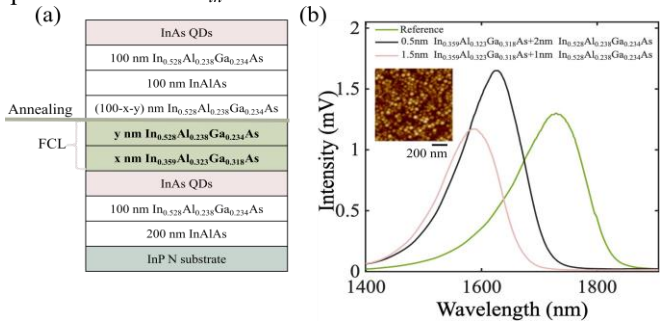

Fig. 2. (a) Schematic structure of single-layer QD sample applying the modified indium flush with different strained FCL. (b) RT PL spectra for single-layer QD samples with different FCL applying modified indium flush. The inset shows 1×1 μm^2 AFM of the uncapped surface dots of the samples.

IV. InAs/InAlGaAs QD Lasers on (001) InP Substrate

Compared with InAs/GaAs QD lasers, the performance of InAs/InAlGaAs QD lasers lags, particularly in terms of low J_{th} and temperature-insensitive operation, mainly due to the severe size/shape inhomogeneity of QDs. To realize high-performance InAs/InAlGaAs QD lasers, achieving uniform QDs with narrow FWHM of PL is critical for enhancing modal gain, low J_{th}, and high-temperature operation. Here, we employed the modified indium flush technique to effectively control dot height and thus obtain high-density and uniform QDs. This approach resulted in InAs/InAlGaAs QD lasers with low threshold and high-temperature operation.

A. 7-stack InAs/InAlGaAs QD laser Growth

The InAs/InAlGaAs QD laser structure was grown on a (001) n-type InP substrate by MBE, and consists of the following layers: Si-doped 200 nm $In_{0.524}Al_{0.476}As$, Si-doped 200 nm $In_{0.528}Al_{0.238}Ga_{0.234}As$, a 7-stack InAs QD active region with optimized growth conditions, Be-doped 200 nm $In_{0.528}Al_{0.238}Ga_{0.234}As$, and Be-doped 200 nm $In_{0.524}AlAs$. A 10 nm Be-doped InGaAs cap was deposited to prevent oxidation during the subsequent transfer to MOCVD, where a Zn-doped 1700 nm InP p-type cladding layer and a Zn-doped 200 nm InGaAs p-contact layer were grown.

Fig. 3 presents HAADF STEM images for the seven-stack QD laser along the (a) [110] and (b) $[1\bar{1}0]$ directions to confirm the dot morphology. The InAs QDs exhibit a truncated lens shape with an average size of 25.7 nm along [110] and 47.3 nm along $[1\bar{1}0]$ direction. Although minor elongation is observed, the nanostructures are distinct from the Qdash that presents continuous-phase InAs layer along the $[1\ \bar{1}\ 0]$ direction resembling a QW [26]. The height along [110] direction is 3.4 nm, slightly higher than 2.9 nm observed along $[1\ \bar{1}\ 0]$, indicating a minor anisotropy. Importantly, the positions of the QDs in each layer are randomly distributed, rather aligned with

the bottom of QDs in layers above or below, evidencing negligible strain coupling effects.

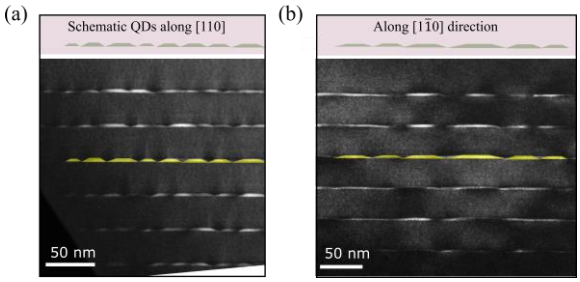

Fig. 3 HAADF images along both (a) [110] and (b) [1$\bar{1}$0] directions of the seven-QD-layer laser on InP substrate and their schematic shapes.

B. Low threshold InAs/InAlGaAs QD lasers

Broad-area FP lasers with a ridge width of 15 μm were first fabricated and tested. The fabricated FP lasers were characterized under pulsed injection (1 % duty cycle, 1 μs pulse width) to minimize the self-heating effect. Fig. 4(a) displays typical power-current (*LI*) curves for varied cavity lengths. The threshold current (I_{th}) and J_{th} for devices with 3000, 2000, 1000, and 500 μm cavity lengths were measured to be 198 mA (440 A/cm^2), 145 mA (483 A/cm^2), 92 mA (613 A/cm^2), and 89 mA (1,189 A/cm^2), respectively. These correspond to J_{th} per QD layer of 63, 69, 88, and 170 A/cm^2. The achieved J_{th} per QD layer of 63 and 69 A/cm^2 for the 3000 and 2000 μm devices outperformed prior reports for C-/L-band InAs/InAlGaAs QD lasers on (001) InP. Fig. 4(b) presents temperature-dependent *LI* characteristics of the 2000 μm device, showing a maximum operating temperature of 130 °C. The inset of Fig. 4(b) depicts J_{th} versus temperature on a logarithm scale, in which the J_{th} increases from 483 A/cm^2 at 20 °C to 6,628 A/cm^2 at 130 °C. The characteristic temperature (T_0), a measure of temperature sensitivity of I_{th} or J_{th} evaluated from $J_{th}(T) = J_0 \times \exp(T/T_0)$, was 48.2 K (below 70 °C) and 44.9 K (above 70 °C). The RT peak lasing wavelength is 1624 nm and the shift rate is 0.37 nm/K. Note that maximum operating temperatures for the 3000, 1000, and 500 μm devices were 110, 120, and 120 °C, respectively (not shown here).

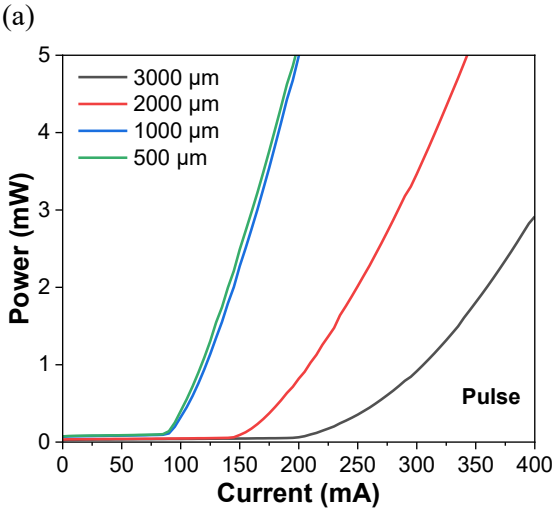

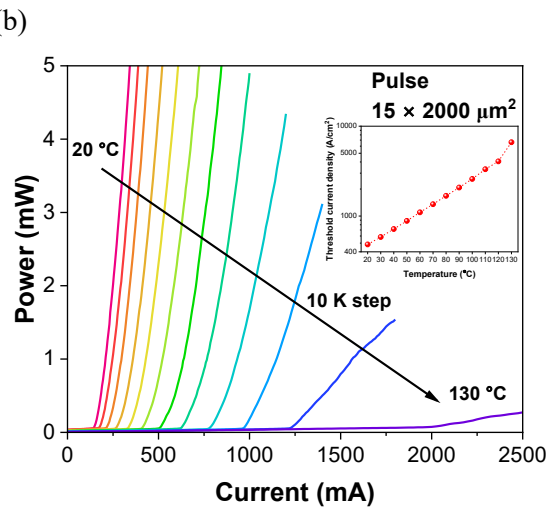

Fig. 4. (a) RT *LI* for the InAs/InAlGaAs QD lasers with cavity width of 15 μm and different cavity lengths. (b) Temperature-dependent *LI* characteristics for the 15 μm × 2000 μm device. The inset presents the J_{th} versus temperature. (Adapted from [52] under CC BY 4.0)

Fig. 5 exhibits continuous-wave (CW) temperature-dependent *LI* curves of the 15 μm × 2000 μm device, confirming a maximum operating temperature of 35 °C. The device yields I_{th} of 393 mA (J_{th} of 1.31 kA/cm^2; 187 A/cm^2 per QD layer), series resistance of 1.6 Ω, and turn-on voltage of ~ 0.7 V. The reduced T_0 of 32 K was evaluated, highlighting the substantial impact of self-heating under CW operation. As shown in the inset of Fig. 5, the RT peak lasing wavelength at an injection current of 1.1 × I_{th} and wavelength shift rate are evaluated as 1631 nm and 0.76 nm/K, respectively.

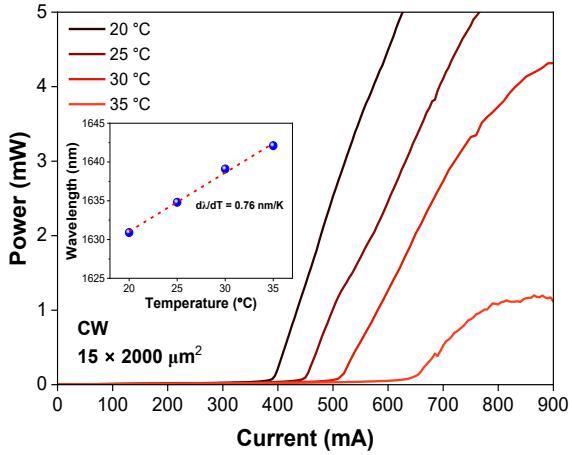

Fig. 5. CW temperature-dependent *LI* characteristics of the 15 μm × 2000 μm device. The inset shows peak lasing wavelength versus temperature.

Low threshold L-band InAs/InAlGaAs QD lasers were demonstrated using the modified indium flush technique. The fabricated seven-stack as-cleaved lasers with a cavity length of 15 μm and cavity lengths of 2000 and 3000 μm under pulsed injection achieved very low J_{th} per QD layer of 63 and 69 A/cm^2

and maximum operating temperature of 110 and 130 °C, respectively. While the pulsed performance is promising, the performance under CW—a J_{th} per QD layer of 187 A/cm^2 and a maximum operating temperature of 35 °C for the 15 × 2000 μm^2 device—is limited, requiring further optimization to enhance CW performance.

C. High-temperature and ultra-short cavity operation of InAs/InAlGaAs QD lasers

To investigate the impact of a reduced ridge width on the temperature stability, narrow-ridge devices with a cavity width of 5 μm were fabricated. Fig. 6 displays pulsed temperature-dependent *LI* curves for the 2000 μm device, yielding I_{th} of 64.3 mA (J_{th} of 643 A/cm^2) and a maximum operating temperature of 140 °C, which is 10 °C higher than the 15 μm × 2000 μm device. T_0 values were 58 K (20 – 70 °C) and 36 K (70 – 140 °C). The enhanced maximum operating temperature for the narrow-ridge device with moderate cavity length of 2000 μm can be attributed primarily to the lower I_{th} compared to the 15 μm ridge device with the same cavity length—namely, less Joule heating. The inset of Fig. 6 shows a lasing wavelength shift with increasing temperature at an injection current of 1.1 × I_{th}. The peak lasing wavelength at RT is centered at 1625 nm and redshifts with a shift rate of 0.39 nm/K. Note that the reduced redshift is observed near the maximum operating temperature, which has also been found in literature [12, 53]. This is believed to be due to high current injection-induced variation in effective refractive index [54]. While the redshift driven by bandgap shrinkage dominates over the carrier-induced blueshift as the temperature increases, an excessively increased J_{th} and reduced quantum efficiency near the maximum operating temperature generate a large amount of unclamped excess carriers, which would mitigate the redshift [55].

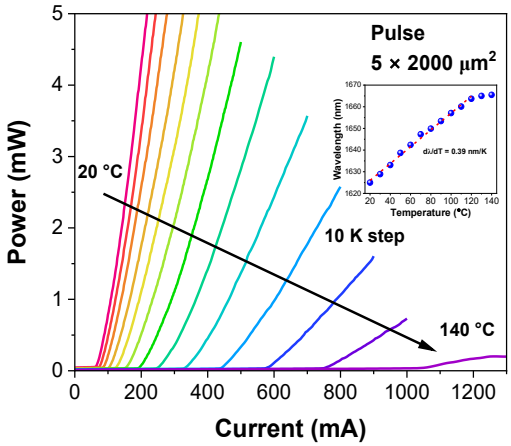

Fig 6. Temperature-dependent *LI* curves under pulsed injection for the 5 μm × 2000 μm device. Temperature-induced lasing wavelength shift is shown in the inset.

The 5 μm × 2000 μm device was further characterized under CW operation. Fig. 7 shows CW temperature-dependent *LI* curves, with a maximum operating temperature of 60 °C, 25 °C higher than the 15 μm × 2000 μm device. The I_{th} (J_{th}) at RT was measured as 137 mA (1.37 kA/cm^2), with a series resistance of 1.6 Ω and turn-on voltage of ~ 0.7 V. The improved T_0 of 40 K was obtained, compared to the 15 μm × 2000 μm device (32.0 K). The inset of Fig. 7 displays a peak lasing wavelength shift at an injection current of 1.1 × I_{th} as a function of temperature. The RT peak lasing wavelength is 1627 nm, and the shift rate is 0.56 nm/K, lower than 0.76 nm/K (15 μm × 2000 μm).

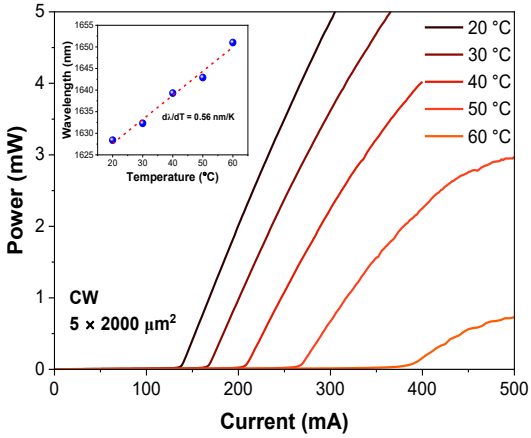

Fig. 7. CW temperature-dependent *LI* characteristics for the 5 × 2000 μm^2 device. Inset presents peak lasing wavelength shift as a function of temperature.

Table I summarizes key performance metrics for the devices with different cavity lengths and widths, in terms of I_{th}, J_{th}, single-facet power, maximum operating temperature, and T_0. For the device with cavity width of 15 μm under pulsed injection, shorter cavity length devices have shown higher maximum operating temperature than longest cavity length (3000 μm) predominantly due to reduction in I_{th} and Joule heating. However, the 1000 and 500 μm devices degraded by 10 °C, compared with the 2000 μm device. This is because the excessive mirror loss in short cavity length significantly increases the J_{th}, thereby resulting in increased non-radiative recombination and thermal carrier escape rate at high temperature regime [52]. In other words, excessively high carrier density in short cavity length diminishes the benefit of lower I_{th} at high temperatures. For the temperature dependence of J_{th}, shorter cavity devices exhibit higher T_0 at lower temperatures but more pronounced degradation in T_0 at higher temperatures. Similar to the operating temperature, this can be attributed to the higher mirror loss and resultant higher carrier density, further enhancing loss mechanism at high temperature range [52]. Compared with the 15 × 2000 μm^2 device, accordingly, the much lower I_{th} contributed to the improved thermal stability of the 5 × 2000 μm^2 device.

However, a notable performance degradation was observed under CW operation compared with pulsed mode, primarily attributed to self-heating, further exacerbated by non-optimal shallow, wet-etched waveguide ridge geometry and defects in the regrown p-InP cladding layer. Adopting a deep, dry-etched ridge waveguide can enhance optical mode confinement and reduce I_{th} [56]. Using monolithic growth to avoid regrowth defects [57] and applying high-reflection facet coatings will

TABLE I

SUMMARY OF DEVICE PERFORMANCE FOR INAS/INALGAAS QD LASERS WITH VARIED CAVITY LENGTHS AND CAVITY WIDTH OF 15 μM AND 5 μM

Current injection	Cavity width	Cavity length	I_{th} (mA)	J_{th} (A/cm^2)	Single facet power (mA) at 0.5 / 1.0 A	Max. temp.	T_0 (< 70 °C)	T_0 (> 70 °C)
Pulse	15 μm	3000 μm	198	440	5.6 / 30	110 °C	44.3 K	41.3 K
		2000 μm	145	483	12 / 48	130 °C	48.2 K	44.9 K
		1000 μm	92	613	22 / 69	120 °C	50.9 K	39.0 K
		500 μm	89	1189	24 / 60	120 °C	55.3 K	37.2 K
	5 μm	2000 μm	64	643	17 / 43	140 °C	58.0 K	36.0 K
CW	15 μm	2000 μm	393	1310	1.5 / 4.7 (at 0.8 A)	35 °C	32 K	-
	5 μm		137	1370	8.4 / 9.3 (at 0.65 A)	60 °C	40 K	-

further improve CW performance. In addition, epi-side-down mounting on high-thermal-conductivity submounts can greatly improve heat dissipation [58]. These strategies can narrow the gap between CW and pulsed operation.

In addition to demonstrating high-temperature operation of InAs/InAlGaAs QD lasers, we investigated the lasing characteristics of short cavity-length devices to explore their potential for high-speed applications. InAs/InAlGaAs QD lasers with cavity lengths less than 500 μm were characterized at RT under pulsed injection.

As shown in Fig. 8(a), the *LI* curves for devices with cavity lengths of 375, 300, 250, 200, and 180 μm reveals I_{th} of 46, 52, 61, 82, and 95 mA, corresponding to J_{th} of 2.4, 3.5, 4.8, 8.2, and 10.6 kA/cm^2, respectively. Notably, even the ultra-short cavity device with a length of 180 μm demonstrated lasing without any facet coating, highlighting the capability of our QD laser structure to support considerably high gain. To the best of our knowledge, this represents the record-short cavity length achieved for C-/L-band InAs/InAlGaAs QD lasers on (001) InP. Fig. 8(b) presents the optical spectra at an injection current of 1.1 × I_{th}. The peak lasing wavelength blue-shifted from 1589 nm (L-band) to 1540 nm (C-band). This shift is primarily ascribed to the higher threshold gain requirement induced by higher mirror losses in shorter cavities, leading to lasing at shorter wavelengths within the QD ensemble where the modal gain is higher [59, 60].

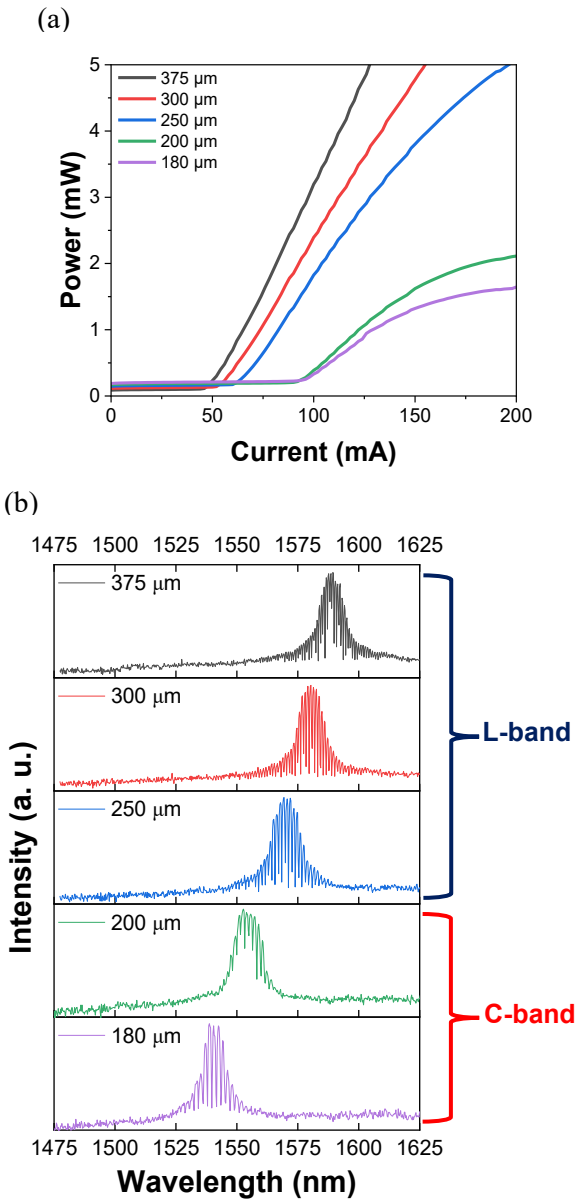

Fig. 8. (a) RT *LI* characteristics for devices with cavity length

This article has been accepted for publication in IEEE Journal of Selected Topics in Quantum Electronics. This is the author's version which has not been fully edited and content may change prior to final publication. Citation information: DOI 10.1109/JSTQE.2025.3641548

less than 500 µm. (b) Optical spectra at an injection current of 1.1 × I_{th} for the short cavity length devices.

Based on the device data with varying cavity lengths and widths, the peak modal gain at threshold was evaluated. The mirror losses for each cavity length were calculated assuming an as-cleaved facet reflectivity of R = 0.32. Internal loss (α_i) and internal quantum efficiency (η_i) were extracted from the dependence of the external differential quantum efficiency on cavity length, using devices with a 5 µm and varied cavity lengths ranging from 500 to 2000 µm. A linear fit to this data yielded η_i of 20 % and α_i of ~ 12 cm^{-1}. Note that the extracted low η_i is likely limited by non-radiative recombination at defects introduced during p-InP regrowth, while α_i is influenced by heterointerface and defect-induced scattering. Future optimization will focus on monolithic MBE growth to reduce these losses. Fig. 9 exhibits the peak modal gain at threshold as a function of current density, calculated from the mirror losses for each cavity length and the evaluated α_i of ~ 12 cm^{-1}. In addition to the 5 µm cavity width devices, data from devices with 15 µm and 50 µm cavity widths and varying cavity lengths were included in the analysis. A high modal gain of 76 cm^{-1} was obtained.

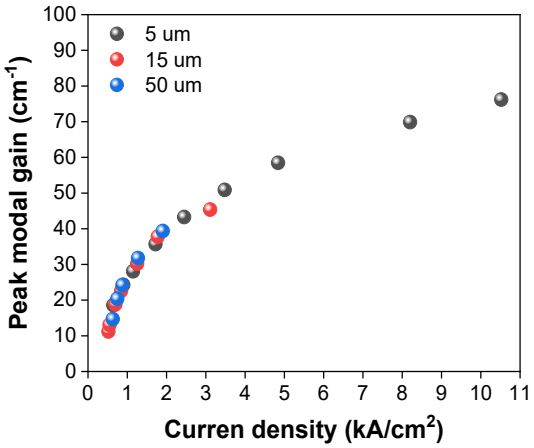

Fig. 9. Peak modal gain versus current density.

V. InAs/InAlGaAs QD Lasers Directly Grown on (001) Si Substrate

Despite the growing demand for C- and L-band Si-based on-chip light sources, progress in developing InAs/InAlGaAs QD lasers directly grown on (001) Si substrates is stagnant. In contrast to the substantial advances achieved with O-band InAs/GaAs QD lasers on Si, the realization of high-performance InAs/InAlGaAs QD lasers remains more challenging. First, the lattice mismatch between InP and Si (~ 8%) is larger than GaAs and Si (~ 4%), generating a much higher density of threading dislocations. Second, the severe size and shape inhomogeneity of InAs QDs grown on InP/Si limits sufficient gain, resulting in higher J_{th} and limited high-temperature operation. Here, Si substrate pre-treatment [61] and InAsP dislocation filters [62] were employed to suppress the formation of antiphase boundaries and reduce threading dislocation density. On a MOCVD-grown InP/Si template, 7-stack InAs/InAlGaAs QD lasers were grown using the modified indium flush technique.

A. 7-stack InAs/InAlGaAs QD lasers growth on Si substrate

Based on the InAs/InAlGaAs QD laser results, an optimized seven-stack InAs/InAlGaAs/InP QD laser structure was further exploited on on-axis Si (001) substrate. First, an InP/GaAs/Si template with a total thickness of 570 nm was grown. The use of a plasma-based surface deoxidization process in conjunction with high-temperature Si annealing result in antiphase boundary-free III-V epitaxial layers [61]. The threading dislocation density of the thin buffer template was measured to be 1.7 × 10^9 cm^{-2}. This dislocation density was further reduced to 6.6 × 10^7 cm^{-2} via two sets of InAsP dislocation filters [62]. The InP/GaAs buffer developed here is considerably thinner than previous work in the literature [42, 63]. Unlike InP-based QD lasers where an n-type InP substrate serves as the n-type contact layer, an undoped (230 nm) and an n-type (770 nm) InP layers were subsequently grown by MOCVD for this role. The InAs/InAlGaAs QDs region was repeated following the previous optimized conditions using the modified indium flush technique in MBE. Finally, the p-type InP cladding and p-InGaAs contact layers were grown by MOCVD to complete the laser structure.

B. Electrically pumped InAs/InAlGaAs QD lasers on Si

7-stack InAs/InAlGaAs QD FP lasers directly grown on (001) Si substrate with ridge widths of 50 µm and 5 µm were fabricated. The FP lasers were characterized under pulsed injection (1 % duty cycle, 1 µm pulse width) to suppress self-heating effect. Typical *LI* characteristics at RT for devices with varied cavity lengths and ridge widths of 50 and 5 µm were measured to evaluate J_{th} trend (not shown). For the broad-area lasers (50 µm ridge width) with cavity lengths of 2000, 1000, 750, 500, and 350 µm, the measured I_{th} were 1353, 694, 666, 576, and 524 mA, corresponding to J_{th} values of 1.35, 1.39, 1.78, 2.30, and 2.79 kA/cm^2, respectively. The narrow-ridge devices (5 µm) with cavity lengths of 2000, 1500, 750, 500, and 375 µm exhibit I_{th} (J_{th}) of 323 (3.23), 262 (3.49), 154 (4.10), 119 (4.76), and 104 mA (5.57 kA/cm^2), respectively. Fig. 10 plots J_{th} versus inverse cavity length for both cavity widths. The extracted transparency current density (J_{tr}) was calculated to be 0.84 and 2.83 kA/cm^2 for the 50 and 5 µm width devices, respectively.

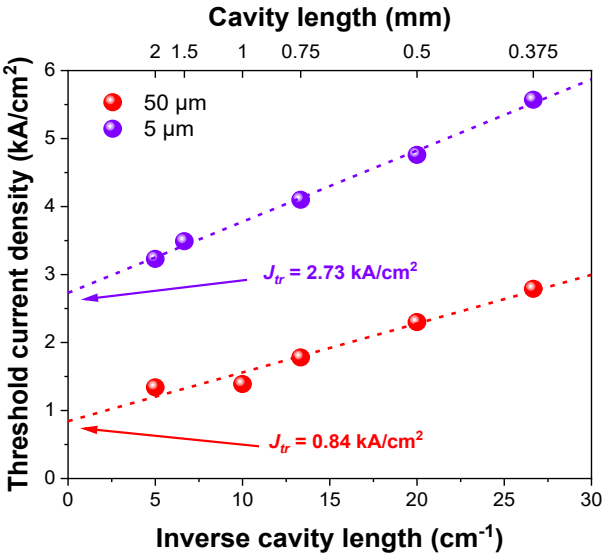

Fig. 10. J_{th} versus inverse cavity length (cavity length) for the 7-stack InAs/InAlGaAs QD lasers on (001) Si with cavity widths of 50 and 5 μm and varied cavity lengths.

To assess the temperature stability of the InAs/InAlGaAs QD lasers on Si, the 5 μm × 2000 μm device was selected for further characterization. Fig. 11(a) presents the temperature-dependent *LI* curves, showing a maximum operating temperature of 100 °C. Note that the RT single-facet power at an injection current of 1 A was measured as 16 mW without showing roll-over. The logarithmic J_{th} versus temperature plot in the inset of Fig. 11(a) exhibits a typical linear relation across the whole temperature range. The characteristic temperatures T_0 and T_1, indicating the temperature dependence of J_{th} and slope efficiency, respectively, were also evaluated, as shown in Fig. 11 (b). The T_0 was extracted as 62.2 K (20 – 100 °C), slightly better than InP-based QD lasers with the same cavity size (58 K below 70 °C and 36 K above 70 °C), due to higher thermal conductivity of Si [64]. On the other hand, the T_1 values were calculated to be 116 K (< 60 °C) and 44 K (> 60 °C). Since the T_1 is sensitive to the conversion efficiency of carriers into photons above threshold, a notable degradation of slope efficiency at higher temperature range is mainly due to the increased thermal carrier escape/leakage and enhanced non-radiative recombination [52].

Fig. 11 (c) displays optical spectra at an injection current of 1.1 × I_{th} as the temperature increases. The ground-state lasing at 1585 nm is observed at RT, and the peak lasing wavelength redshifts to 1620 nm at 100 °C, without switching to the excited-state lasing. The corresponding redshift rate was determined to be 0.45 nm/K, as shown in the inset of Fig. 10 (d).

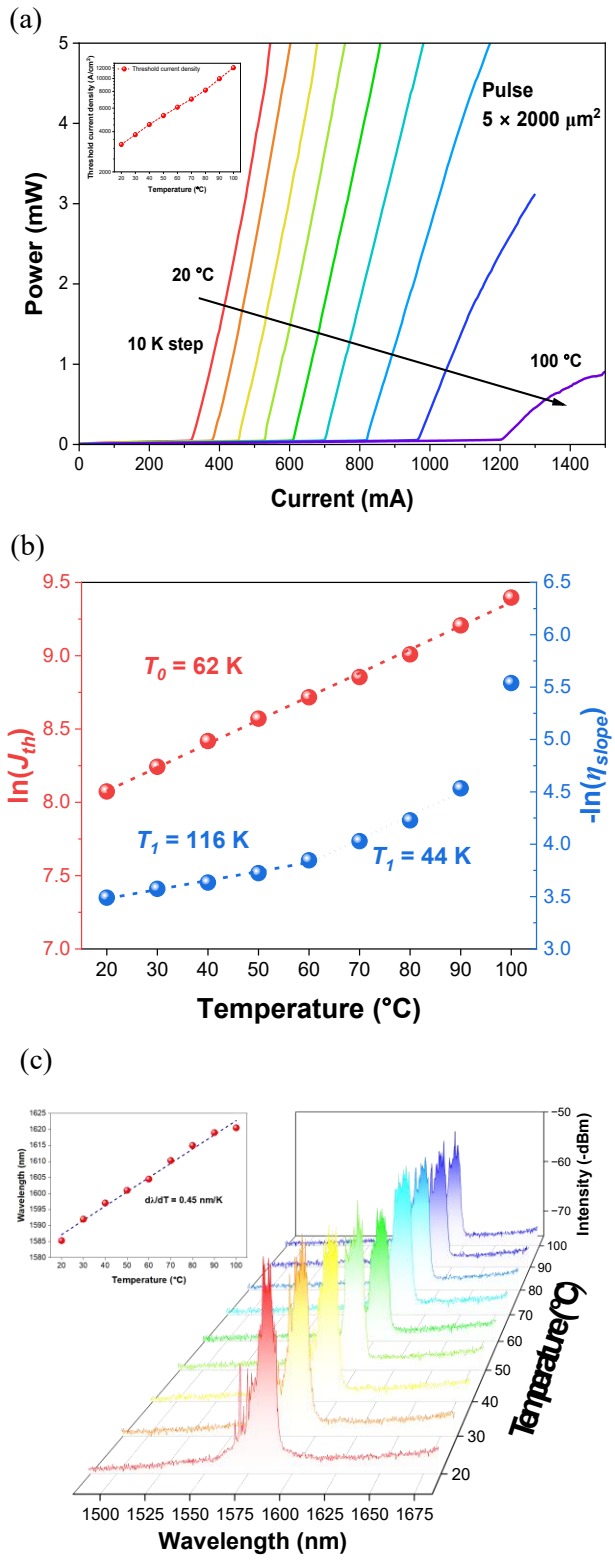

Fig. 11. (a) Temperature-dependent *LI* curves for the 5 μm × 2000 μm device. The temperature-dependent J_{th} is shown in the inset. (b) Characteristic temperatures T_0 and T_1 (c) Optical spectra at an injection current of 1.1 × I_{th} in a temperature range of 20 – 100 °C. The inset displays the temperature-induced peak lasing wavelength shift.

VI. Conclusion

This work presents a comprehensive advancement of InAs/InAlGaAs QD lasers on both InP and Si substrates, enabled by the development of a new capping technique to QDs. By introducing a strained partial capping layer during QD growth, we achieved high-density and uniform QDs with reduced height dispersion and emission wavelength tuning, supporting multi-stack InAs/InAlGaAs/InP QD active region with suppressed strain coupling. By employing this approach, 7-stack InAs/InAlGaAs/InP QD lasers on InP exhibit a record-low J_{th} of 63 A/cm^2 per QD layer (15 × 3000 μm^2) and a maximum operating temperature of 140 °C (5 × 2000 μm^2) under pulsed injection. Under CW operation, the 5 × 2000 μm^2 device achieved a maximum operating temperature of 60 °C, underscoring the need for further thermal and structural optimization. Furthermore, we also achieved electrically injected InAs/InAlGaAs QD lasers directly grown on CMOS-compatible Si (100) substrate, with a low J_{th} of 1.35 kA/cm^2 (50 × 2000 μm^2) and a maximum operating temperature of 100 °C (5 × 2000 μm^2). These results highlight the potential of the InAs/InAlGaAs QD laser as off-chip or on-chip light sources for optical communication and Si photonics, and mark significant progress toward monolithic integration of long-wavelength QD lasers.

References

[1] M. Cantono, R. Schmogrow, M. Newland, V. Vusirikala, and T. Hofmeister, "Opportunities and challenges of C+ L transmission systems," *Journal of Lightwave Technology,* vol. 38, no. 5, pp. 1050-1060, 2020.

[2] T. Sakamoto *et al.*, "Wide wavelength band (1535–1560 nm and 1574–1600 nm), 28× 10 Gbit/s WDM transmission over 320 km dispersion-shifted fibre," *Electronics Letters,* vol. 34, no. 4, pp. 392-394, 1998.

[3] S. Banyoudeh *et al.*, "Temperature-Insensitive High-Speed Directly Modulated 1.55-μm Quantum Dot Lasers," *IEEE Photonics Technology Letters,* vol. 28, no. 21, pp. 2451-2454, 2016.

[4] J. Sun *et al.*, "High-power, electrically-driven continuous-wave 1.55-μm Si-based multi-quantum well lasers with a wide operating temperature range grown on wafer-scale InP-on-Si (100) heterogeneous substrate," *Light: Science & Applications,* vol. 13, no. 1, p. 71, 2024.

[5] P. Baziana, G. Drainakis, D. Georgantas, and A. Bogris, "AI and ML Applications Traffic: Designing Challenges for Performance Optimization of Optical Data Center Networks," in *2024 International Conference on Software, Telecommunications and Computer Networks (SoftCOM)*, 2024: IEEE, pp. 1-6.

[6] S. Bauer *et al.*, "1.5-μm indium phosphide-based quantum dot lasers and optical amplifiers: The impact of atom-like optical gain material for optoelectronics devices," *IEEE Nanotechnology Magazine,* vol. 15, no. 2, pp. 23-36, 2021.

[7] Y. Arakawa and H. Sakaki, "Multidimensional quantum well laser and temperature dependence of its threshold current," *Applied physics letters,* vol. 40, no. 11, pp. 939-941, 1982.

[8] K. Nishi, K. Takemasa, M. Sugawara, and Y. Arakawa, "Development of quantum dot lasers for data-com and silicon photonics applications," *IEEE Journal of Selected Topics in Quantum Electronics,* vol. 23, no. 6, pp. 1-7, 2017.

[9] M. Asada, Y. Miyamoto, and Y. Suematsu, "Gain and the threshold of three-dimensional quantum-box lasers," *IEEE Journal of quantum electronics,* vol. 22, no. 9, pp. 1915-1921, 1986.

[10] Y. Wan, J. Norman, S. Liu, A. Liu, and J. E. Bowers, "Quantum dot lasers and amplifiers on silicon: recent advances and future developments," *IEEE Nanotechnology Magazine,* vol. 15, no. 2, pp. 8-22, 2021.

[11] J.-S. Park *et al.*, "High operating temperature (> 200° C) InAs/GaAs quantum-dot laser with co-doping technique," *Journal of Physics D: Applied Physics,* vol. 58, no. 18, p. 185101, 2025.

[12] H. Deng *et al.*, "1.3 μm InAs/GaAs quantum‐dot lasers with p‐type, n‐type, and co‐doped modulation," *Advanced Physics Research,* vol. 3, no. 10, p. 2400045, 2024.

[13] H. Liu *et al.*, "Improved performance of 1.3 μm multilayer InAs quantum-dot lasers using a high-growth-temperature GaAs spacer layer," *Applied Physics Letters,* vol. 85, no. 5, pp. 704-706, 2004.

[14] T. W. Berg, S. Bischoff, I. Magnusdottir, and J. Mork, "Ultrafast gain recovery and modulation limitations in self-assembled quantum-dot devices," *IEEE Photonics Technology Letters,* vol. 13, no. 6, pp. 541-543, 2001.

[15] S. Chen *et al.*, "Electrically pumped continuous-wave III–V quantum dot lasers on silicon," *Nature photonics,* vol. 10, no. 5, pp. 307-311, 2016.

[16] A. D. Lee, Q. Jiang, M. Tang, Y. Zhang, A. J. Seeds, and H. Liu, "InAs/GaAs quantum-dot lasers monolithically grown on Si, Ge, and Ge-on-Si substrates," *IEEE Journal of Selected Topics in Quantum Electronics,* vol. 19, no. 4, pp. 1901107-1901107, 2013.

[17] Y. Han, H. Park, J. Bowers, and K. M. Lau, "Recent advances in light sources on silicon," *Advances in Optics and Photonics,* vol. 14, no. 3, pp. 404-454, 2022.

[18] C. Shang *et al.*, "Electrically pumped quantum-dot lasers grown on 300 mm patterned Si photonic wafers," *Light: Science & Applications,* vol. 11, no. 1, p. 299, 2022.

[19] V. Khatri, V. Sichkovskyi, L. Popilevsky, Y. Kauffmann, G. Eisenstein, and J. P. Reithmaier, "Increased Modal Gain in 1.55 μm Quantum Dot Lasers Based on Improved Size Homogeneity Obtained by Comprehensive Growth Optimization," *ACS Photonics,* 2025.

[20] H. Lan and Y. Ding, "Ordering, positioning and uniformity of quantum dot arrays," *Nano today,* vol. 7, no. 2, pp. 94-123, 2012.

[21] M. Cotta *et al.*, "Kinetic surface roughening in molecular beam epitaxy of InP," *Physical review letters,* vol. 70, no. 26, p. 4106, 1993.

[22] C. Paranthoen *et al.*, "Height dispersion control of InAs/InP quantum dots emitting at 1.55 μm," *Applied Physics Letters,* vol. 78, no. 12, pp. 1751-1753, 2001.

[23] S. Fathpour, Z. Mi, and P. Bhattacharya, "High-speed quantum dot lasers," *Journal of Physics D: Applied Physics,* vol. 38, no. 13, p. 2103, 2005.

[24] S. Banyoudeh and J. P. Reithmaier, "High-density 1.54 μm InAs/InGaAlAs/InP (100) based quantum dots with reduced size inhomogeneity," *Journal of Crystal Growth,* vol. 425, pp. 299-302, 2015.

[25] C. Gilfert, E.-M. Pavelescu, and J. Reithmaier, "Influence of the As2/As4 growth modes on the formation of quantum dot-like InAs islands grown on InAlGaAs/InP (100)," *Applied Physics Letters,* vol. 96, no. 19, 2010.

[26] D. Jung, D. J. Ironside, S. R. Bank, A. C. Gossard, and J. E. Bowers, "Effect of growth interruption in 1.55 μm InAs/InAlGaAs quantum dots on InP grown by molecular beam epitaxy," *Journal of Applied Physics,* vol. 123, no. 20, 2018.

[27] J. Brault, M. Gendry, G. Grenet, G. Hollinger, Y. Desieres, and T. Benyattou, "Role of buffer surface morphology and alloying effects on the properties of InAs nanostructures grown on InP (001)," *Applied physics letters,* vol. 73, no. 20, pp. 2932-2934, 1998.

[28] J. S. Kim, J. H. Lee, S. U. Hong, W. S. Han, H.-S. Kwack, and D. K. Oh, "Effects of a thin InGaAs layer on InAs quantum dots embedded in InAl (Ga) As," *Applied physics letters,* vol. 83, no. 18, pp. 3785-3787, 2003.

[29] S. Anantathanasarn, R. Nötzel, P. Van Veldhoven, T. Eijkemans, and J. Wolter, "Wavelength-tunable (1.55‐μm region) InAs quantum dots in InGaAsP／InP (100) grown by metal-organic vapor-phase epitaxy," *Journal of applied physics,* vol. 98, no. 1, 2005.

[30] Q. Gong, R. Nötzel, P. Van Veldhoven, T. Eijkemans, and J. Wolter, "Wavelength tuning of InAs quantum dots grown on InP (100) by chemical-beam epitaxy," *Applied Physics Letters,* vol. 84, no. 2, pp. 275-277, 2004.

[31] S. Bhowmick, M. Z. Baten, T. Frost, B. S. Ooi, and P. Bhattacharya, "High Performance InAs/$In_{0.53}Ga_{0.23}Al_{0.24}As$/InP Quantum Dot 1.55 μm Tunnel Injection Laser," *IEEE Journal of Quantum Electronics,* vol. 50, no. 1, pp. 7-14, 2013.

[32] X. Yu *et al.*, "Optically enhanced single-and multi-stacked 1.55 μm InAs/InAlGaAs/InP quantum dots for laser applications," *Journal of Physics D: Applied Physics,* vol. 56, no. 28, p. 285101, 2023.

[33] D. Zhou *et al.*, "Low threshold current density of InAs quantum dash laser on InP (100) through optimizing double cap technique," *Applied Physics Letters,* vol. 94, no. 8, 2009.

[34] S. Luo, H.-M. Ji, X.-G. Yang, and T. Yang, "Impact of double-cap procedure on the characteristics of InAs/InGaAsP/InP quantum dots

grown by metal-organic chemical vapor deposition," *Journal of crystal growth,* vol. 375, pp. 100-103, 2013.

[35] B. Shi and K. M. Lau, "Enhanced optical properties of InAs/InAlGaAs/InP quantum dots grown by metal-organic chemical vapor deposition using a double-cap technique," *Journal of Crystal Growth,* vol. 433, pp. 19-23, 2016.

[36] J. Ulloa, P. Koenraad, E. Gapihan, A. Letoublon, and N. Bertru, "Double capping of molecular beam epitaxy grown InAs ⁄ InP quantum dots studied by cross-sectional scanning tunneling microscopy," *Applied Physics Letters,* vol. 91, no. 7, 2007.

[37] B. Wang *et al.*, "InAs quantum dots with a narrow photoluminescence linewidth for a lower threshold current density in 1.55 μm lasers," *Optical Materials Express,* vol. 14, no. 4, pp. 1074-1084, 2024.

[38] C. Shang *et al.*, "High-temperature reliable quantum-dot lasers on Si with misfit and threading dislocation filters," *Optica,* vol. 8, no. 5, pp. 749-754, 2021.

[39] J. C. Norman, R. P. Mirin, and J. E. Bowers, "Quantum dot lasers—History and future prospects," *Journal of Vacuum Science & Technology A,* vol. 39, no. 2, 2021.

[40] J.-S. Park, M. Tang, S. Chen, and H. Liu, "Heteroepitaxial growth of III-V semiconductors on silicon," *Crystals,* vol. 10, no. 12, p. 1163, 2020.

[41] M. Tang *et al.*, "Integration of III-V lasers on Si for Si photonics," *Progress in Quantum Electronics,* vol. 66, pp. 1-18, 2019.

[42] S. Zhu, B. Shi, Q. Li, and K. M. Lau, "1.5 μm quantum-dot diode lasers directly grown on CMOS-standard (001) silicon," *Applied Physics Letters,* vol. 113, no. 22, 2018.

[43] B. Shi, Y. Han, Q. Li, and K. M. Lau, "1.55-μm lasers epitaxially grown on silicon," *IEEE Journal of Selected Topics in Quantum Electronics,* vol. 25, no. 6, pp. 1-11, 2019.

[44] Z. Wasilewski, S. Fafard, and J. McCaffrey, "Size and shape engineering of vertically stacked self-assembled quantum dots," *Journal of crystal growth,* vol. 201, pp. 1131-1135, 1999.

[45] S. Fafard, Z. Wasilewski, C. N. Allen, K. Hinzer, J. McCaffrey, and Y. Feng, "Lasing in quantum-dot ensembles with sharp adjustable electronic shells," *Applied physics letters,* vol. 75, no. 7, pp. 986-988, 1999.

[46] H. Sasakura, S. Kayamori, S. Adachi, and S. Muto, "Effect of indium-flush method on the control of photoluminescence energy of highly uniform self-assembled InAs quantum dots by slow molecular beam epitaxy growth," *Journal of applied physics,* vol. 102, no. 1, 2007.

[47] J. Yuan *et al.*, "Indium-flush technique for C-band InAs/InP quantum dots," *APL Materials,* vol. 12, no. 12, 2024.

[48] S. Haffouz *et al.*, "Growth and fabrication of quantum dots superluminescent diodes using the indium-flush technique: A new approach in controlling the bandwidth," *Journal of crystal growth,* vol. 311, no. 7, pp. 1803-1806, 2009.

[49] J. Kwoen, M. Kakuda, and Y. Arakawa, "Wide-range emission wavelength control of InAs quantum dots by changing the indium composition in an InAlGaAs capping layer," *Optical Materials Express*, vol. 15, no. 4, pp. 939-948, 2025.

[50] J. Kwoen, J. Jung, M. Kakuda, and Y. Arakawa, "C‐band All III‐Arsenide InAs Quantum Dot Lasers on InP Using Low Indium Composition Partial Capping," *Electronics Letters,* vol. 61, no. 1, p. e70308, 2025.

[51] K. Akahane, N. Yamamoto, and M. Tsuchiya, "Highly stacked quantum-dot laser fabricated using a strain compensation technique," *Applied Physics Letters,* vol. 93, no. 4, p. 041121, 2008.

[52] J.-S. Park *et al.*, "Low threshold InAs/InP quantum dot lasers," *Optics Express,* vol. 33, no. 9, pp. 19158-19165, 2025.

[53] V. Sichkovskyi, M. Waniczek, and J. Reithmaier, "High-gain wavelength-stabilized 1.55 μm InAs/InP (100) based lasers with reduced number of quantum dot active layers," *Applied Physics Letters,* vol. 102, no. 22, p. 221117, 2013.

[54] B. R. Bennett, R. A. Soref, and J. A. Del Alamo, "Carrier-induced change in refractive index of InP, GaAs and InGaAsP," *IEEE Journal of Quantum Electronics,* vol. 26, no. 1, pp. 113-122, 1990.

[55] K. Murasawa, T. Hidaka, and K. Sato, "Injection-current-induced blue-shift laser diode: concept of excess carrier conservation," *Japanese Journal of Applied Physics,* vol. 50, no. 4R, p. 042101, 2011.

[56] Y. Xue, W. Luo, S. Zhu, L. Lin, B. Shi, and K. M. Lau, "1.55 μm electrically pumped continuous wave lasing of quantum dash lasers grown on silicon," *Optics Express* vol. 28, no. 12, pp. 18172-18179, 2020.

[57] Y. Takino, M. Shirao, T. Sato, N. Nishiyama, T. Amemiya, and S. Arai. "Regrowth interface quality dependence on thermal cleaning of AlGaInAs/InP buried-heterostructure lasers," *Japanese journal of applied physics* vol. 50, no. 7R, pp. 070203, 2011.

[58] X. Liu, M. H. Hu, H. K. Nguyen, C. G. Caneau, M. H. Rasmussen, R. W. Davis, and C. Zah. "Comparison between epi-down and epi-up bonded high-power single-mode 980-nm semiconductor lasers," *IEEE Transactions on Advanced Packaging* vol. 27, no. 4, pp. 640-646, 2004.

[59] F. Klopf, S. Deubert, J. Reithmaier, and A. Forchel, "Correlation between the gain profile and the temperature-induced shift in wavelength of quantum-dot lasers," *Applied Physics Letters,* vol. 81, no. 2, pp. 217-219, 2002.

[60] R. Debusmann, T. W. Schlereth, S. Gerhard, W. Kaiser, S. Hofling, and A. Forchel, "Gain studies on quantum-dot lasers with temperature-stable emission wavelength," *IEEE Journal of Quantum Electronics,* vol. 44, no. 2, pp. 175-181, 2008.

[61] R. Alcotte *et al.*, "Epitaxial growth of antiphase boundary free GaAs layer on 300 mm Si (001) substrate by metalorganic chemical vapour deposition with high mobility," *APL Materials,* vol. 4, no. 4, p. 046101, 2016.

[62] S. Liu *et al.*, "Effective InAsP dislocation filtering layers for InP heteroepitaxy on CMOS-standard (001) silicon," *Applied Physics Letters,* vol. 125, no. 8, p. 082102, 2024.

[63] B. Shi, H. Zhao, L. Wang, B. Song, S. T. Suran Brunelli, and J. Klamkin, "Continuous-wave electrically pumped 1550 nm lasers epitaxially grown on on-axis (001) silicon," *Optica,* vol. 6, no. 12, pp. 1507-1514, 2019.

[64] A. Thiam, Y. Roelens, C. Coinon, V. Avramovic, B. Grandchamp, D. Ducatteau, X. Wallart, C. Maneux, and M. Zaknoune. "InP HBT thermal management by transferring to high thermal conductivity silicon substrate," *IEEE Electron Device Letters* vol. 35, no. 10, pp. 1010-1012, 2014.

Hui Jia received the Ph.D. degree in electronic and electrical engineering from University College London (UCL), U.K. in 2023.

She became a Research Associate in the Molecular Beam Epitaxy (MBE) Lab at UCL after receiving the Ph.D. degree. Her research interest includes the epitaxial growth of low-dimensional III-V and Group-IV semiconductors by MBE for Si Photonics.

Jae-Seong Park received B.Sc. (2010), M.Eng. (2012), and Ph.D. (2016) degrees in Materials Science and Engineering from Korea University, South Korea. In 2017, he joined the Molecular Beam Epitaxy group in the Department of Electronic and Electrical Engineering at University College London (UCL), United Kingdom. His research focuses on the epitaxial growth of low-dimensional III-V semiconductors and the development of quantum dot optoelectronic devices based on GaAs, InP, and Si.

Jun Li began his Ph.D. studies in August 2013 and is currently a Ph.D. candidate at University College London, London, U.K. His research focuses on the direct molecular beam epitaxy growth of 1.3 μm and 1.5 μm InAs quantum dot lasers on patterned on-axis silicon substrates. His work addresses laser integration for silicon photonics and the suppression of defects in III–V/Si epitaxy.

Kongming Liu received the M.Eng. degree in and electrical engineering from University College London (UCL), London, in 2024. He is currently pursuing the Ph.D. degree in Electronic and Electrical Engineering at UCL.

From 2024, he is a Ph.D. student at Molecular Beam Epitaxy Group at UCL. His research interest includes the C-band Quantum Dot Laser on InP substrate and patterned silicon substrate.

This article has been accepted for publication in IEEE Journal of Selected Topics in Quantum Electronics. This is the author's version which has not been fully edited and content may change prior to final publication. Citation information: DOI 10.1109/JSTQE.2025.3641548

Jiajing Yuan received the M.Eng. degree in electronic and electrical engineering from University College London (UCL), London, U.K., in 2021. In 2022, she joined the Molecular Beam Epitaxy Laboratory at UCL as a Ph.D. candidate. Her current research focuses on the growth and characterization of InAs/InP quantum dot lasers for photonic integration.

Calum Dear received his B.Sc. in physics in 2020, followed by an M.Sc. in compound semiconductor physics in 2021, both from Cardiff University, Wales, United Kingdom. In 2021, he joined the Molecular Beam Epitaxy Group in the Department of Electronic and Electrical Engineering at University College London, United Kingdom, to pursue a Ph.D. in electronic and electrical engineering.

His Ph.D. research focuses on the epitaxial growth of high-density, high-uniformity III-V quantum dot materials emitting in the C- and L-bands, as well as laser device fabrication.

Haotian Zeng holds B.Eng., M.Eng., and Ph.D. degrees from the MBE Group in the Department of Electrical and Electronic Engineering at University College London, UK, awarded in 2016, 2017, and 2022, respectively. He is currently a Research Associate at University College London. His research interests focus on the growth of III–V nanowires using molecular beam epitaxy and the fabrication of III–V optoelectronic devices.

Yangqian Wang received the B.Eng. and M.S. degree in microelectronics and solid-state electronics in China. She is currently a Ph.D. degree candidate at University College London fully funded by EPSRC CDT in Compound Semiconductor Manufacturing. Her current research interest is the development of mid-infrared InP- /Si- based InAs quantum dot lasers.

Khalil El Hajraoui is a staff scientist at the SuperSTEM Laboratory, UK. After a Master and a PhD degree in physics in France, he moved to Portugal where he did a postdoctoral at the International Iberian Nanotechnology Laboratory (INL) in Braga. Both his PhD and postdoctoral work focused on combining high spatial and temporal resolution to correlate structural to electrical properties of semiconducting materials using in-situ heating and biasing scanning transmission electron microscopy.

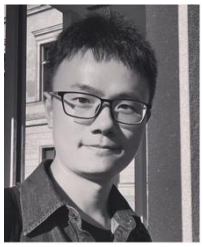

Shangfeng Liu received his B.S. degree in microelectronics and engineering from Sichuan University, Chengdu, China, in 2017, and his Ph.D. degree in condensed matter physics from Peking University, Beijing, China, in 2022.

From 2022 to 2024, he was a postdoctoral research associate at the School of Physics and Astronomy, Cardiff University, United Kingdom. Since 2024, he has been an assistant professor with the School of Physical Science, Great Bay University, Guangdong, China. His research interests focus on the MOCVD epitaxy of group-III nitrides and their applications in power electronics and optoelectronic devices. He has published nearly 30 research papers and holds 14 invention patents.

Huiwen Deng received the B.S. degree in optoelectronic information engineering from Huazhong University of Science and Technology, Wuhan, China, in 2016 and the M.S. Degree in communication and signal processing from Imperial College London, London, UK, in 2017 and the Ph.D. degree in photonics from University College London, London, UK, in 2024. He is currently the lab manager of the UCL MBE lab. He worked extensively in the field of low-dimensional III-V monolithically grown on native substrates and IV platform.

Mickael Martin earned his B.Sc. in physics and M.S. in materials engineering from Strasbourg University, France, in 2001 and 2003, respectively.

In 2011, he joined the Microelectronics Technology Laboratory (CNRS-LTM) at Université Grenoble-Alpes, Grenoble, France. He is currently a process engineer in the Nanomaterials Team, focusing on III-V-on-silicon MOCVD epitaxy for electronic and photonic applications.

Yaonan Hou received the Ph.D. degree in condensed matter physics from Institute of Physics, Chinese Academy of Sciences, Beijing, China, in 2012. He is currently a Senior Lecturer (Associate Professor) leading the research in solid-state compound semiconductor optoelectronics and photonics at the Department of Electronic and Electrical Engineering in Swansea University, UK.

During 2012 and 2017, he worked as a Research Associate in III-V Nitride optoelectronic devices at the University of Sheffield. In 2017-18, he initiated his research in silicon photonics and subsequently joined the Optoelectronics Research Centre (ORC) at the University of Southampton in 2019, working on the on-chip III-V quantum dot lasers integrated with silicon photonic components.

His research focuses on developing novel optoelectronic devices (such as lasers, light-emitting diodes, single photon emitters, photodetectors and PV devices) from broad semiconductor materials, including III-Vs (GaN, GaAs, InP), Oxides (Ga2O3 and ZnO), and group IV materials (Si-Ge-Sn). He is interested in assembling photonic devices on a chip to realize integrated photonic circuits for desired functions.

Quentin Ramasse received an MEng from the Ecole Centrale Paris (France) and a MMaths from the University of Cambridge, where he also obtained his Ph.D. in Physics in 2005 working on optical aberration measurements methodologies for aberration-corrected STEM.

He held a Staff Scientist position from 2005 to 2010 at the National Center for Electron Microscopy (NCEM) in Berkeley, a U.S. Department of Energy-funded user facility where he took part in the TEAM project. He is now the Director of the SuperSTEM Laboratory, the UK National Research Facility for Advanced Electron Microscopy, and holds the Chair of Advanced Electron Microscopy jointly at the School of Chemical and Process Engineering and the School of Physics and Astronomy, University of Leeds, U.K. As the director of SuperSTEM for the last 15 years, Quentin has masterminded the facility's adoption of emerging technologies for the benefit or its user community, commissioning for instance one of the first meV-capable instrument in the world. He has pioneered single-atom core-loss and vibrational spectroscopy, nanoscale momentum-resolved EELS and real-space orbital mapping in the STEM.

Quentin Ramasse was awarded the 2020 Royal Microscopical Society Mid-Career Scientific Achievement Award and is the 2024 recipient of the European Microscopy Society Award for Physical Sciences, which highlighted his contributions to the development of advanced electron microscopy.

Qiang Li received the B.S. degree in microelectronics from Peking University, Beijing, China, in 2009 and the Ph.D. degree in electronic and computer engineering from the Hong Kong University of Science and Technology, Hong Kong, in 2014.

From 2015 to 2018, he was a Research Assistant Professor with the Department of Electronic and Computer Engineering, the Hong Kong University of Science and Technology. Since 2018, he has been with the School of Physics and Astronomy, Cardiff University, Cardiff, United Kingdom, first as a Lecturer and now a Reader. He has published more than 60 journal articles. His research interests include MOCVD epitaxy of quantum dot lasers for optical communications, advanced

III-V epitaxy for Si photonics, type-II superlattice infrared detectors, and nanowire lasers.

Thierry Baron received his Ph.D. in physical sciences from Université Grenoble Alpes in 1996. He began his career as a Postdoctoral Researcher at Universität Würzburg and CEA-Leti before joining CNRS in 1998 as a Research Scientist. Since 2010, he has held the position of Director of Research. From 2016 to 2023, he served as Director of the Laboratoire des Technologies de la Microélectronique (LTM) and co-directed a 700 m^2 nanofabrication cleanroom. He has authored or co-authored more than 300 publications, including journal articles, conference papers, and patents. Currently, he is Senior Researcher at LTM and Director of the LabEx Microelectronics at Université Grenoble Alpes, advancing microelectronics research and innovation.

Mingchu Tang (IEEE Member) is a Lecturer in Molecular Beam Epitaxy within the Department of Electronic and Electrical Engineering at University College London (UCL). He earned his B.Eng. in electronic & electrical engineering from the University of Sussex in 2011 and completed an M.S. in nanotechnology at UCL in 2012. In October 2012, Dr Tang joined UCL's Photonics Group as a Ph.D. candidate, focusing on the molecular beam epitaxial growth of III–V compound semiconductors and their integration into optoelectronic devices. He was awarded his Ph.D. in 2016. Dr Tang's research expertise lies in the epitaxial growth and monolithic integration of III–V quantum dot structures on both III–V and Group IV substrates, with applications in lasers, detectors, and solar cells.

Alwyn Seeds (F 1997) holds the B.Sc, Ph.D. and D.Sc. degrees of the University of London.

After working as a Staff Member at Lincoln Laboratory, Massachusetts Institute of Technology and as Lecturer in Telecommunications at Queen Mary College, University of London, he joined University College London in 1986, where he is currently Professor of Opto-electronics, Head of the Photonics Group and Director of the EPSRC National Dark Fibre Facility. He has more than 20 patents and has published more than 500 papers on microwave and opto-electronic devices and their systems applications, of which some 100 have been invited.

Professor Seeds is a Fellow of the Royal Academy of Engineering (UK), an IEEE Life Fellow (USA) and has served as Vice-President for Technical Affairs of the IEEE Photonics Society (USA). He co-founded Zinwave, a manufacturer of wireless over fibre systems, now a unit of Wilson Electronics LLC. There are now over 850 Zinwave systems installed in 26 countries worldwide. Alwyn Seeds was awarded the Gabor Medal and Prize of the Institute of Physics in 2012, the Distinguished Educator Award of the IEEE Microwave Theory and Techniques Society in 2018 and the Engineering Achievement Award of the IEEE Photonics Society in 2023.

Huiyun Liu received the Ph.D. degree in semiconductor science from the Institute of Semiconductor, Chinese Academy of Sciences. After receiving the Ph.D. degree, he joined the EPSRC National Centre for III–V Technologies at University of Sheffield in August 2001. In 2007, he was awarded Royal Society University Research Fellow and joined the Department of Electronic and Electrical Engineering, University College London, UK, where he is currently a Professor of Semiconductor Photonics. His current research interests encompass the nanoscale engineering of low-dimensional semiconductor structures utilizing Molecular Beam Epitaxy, with a focus on the development of novel optoelectronic devices such as lasers, detectors, solar cells, and modulators. He has authored over 500 scientific papers and holds several patents in the fields of Silicon Photonics and quantum dot technology.